JOURNAL OF SOLID STATE CHEMISTRY 58, 312–324 (1985)

Preparation and Electron Microscopy of Intermediate Phases in the Interval Ce_7O_{12}–$Ce_{11}O_{20}$

PETER KNAPPE* AND LEROY EYRING†

Department of Chemistry and the Center for Solid State Science, Arizona State University, Tempe, Arizona 85287

Received July 24, 1984; in revised form December 26, 1984

Crystals of CeO_2, grown from a flux of sodium tetraborate, were reduced in dry hydrogen to compositions in the interval $CeO_{1.714}$–$CeO_{1.818}$. Selected compositions were studied using a high-resolution electron microscope. The phase $CeO_{1.714}$ (Ce_7O_{12}) was confirmed to have the same unit cell as does Pr_7O_{12} and Tb_7O_{12}. $CeO_{1.818}$ ($Ce_{11}O_{20}$) was found to be isostructural with $Tb_{11}O_{20}$. Two new phases in the interval were established unequivocally. One of them, probably $Ce_{19}O_{34}$, is triclinic with $a = 6.627$, $b = 11.478$, $c = 10.123$, $\alpha = 100.9$, $\beta = 90.0$, and $\gamma = 95.5$, has not previously been observed in any rare earth oxide system. Another, $Ce_{62}O_{112}$, appears to be isomorphous with $Tb_{62}O_{112}$. The two intermediate phases previously reported in this interval, Ce_9O_{16} and $Ce_{10}O_{18}$, were not observed, nor was $Ce_{12}O_{22}$. Diffraction evidence also points to three additional phases in the interval not previously seen.

Introduction

Aside from the intrinsic scientific interest in the phase relationships of the $CeO_{2-\delta}$–O_2 system there is an immense practical interest due to the many uses to which this material is put both in a pure and doped state. Few systems have received more attention with respect to their phase relationships and the nature of the defects caused by the loss of oxygen from the parent fluorite, CeO_2. Suffice it to say that over the years successive phase diagrams have become more and more complex and the models for the defects have come to be considered some types of oxygen vacancies or vacancy cluster complexes (*1–5*).

In recent years the technique of HRTEM has shed a great deal of light on the phase relationships in the analogous systems PrO_x–O_2 and TbO_x–O_2 (*6–8*). All three higher oxide systems exhibit a homologous series of intermediate oxides having the generic compositional formula R_nO_{2n-2}, admitting some exceptions. As between the PrO_x and TbO_x systems the compositional isomerism is not matched in their structures. Although the prototypic phase R_7O_{12} appears to be isostructural in the three cases (*8–10*), polymorphism is the rule.

Until now only neutron and X-ray diffraction techniques have been utilized to investigate the structures in the CeO_x system and these have left much uncertainty. Table I summarizes some results of these studies and Fig. 1 incorporates most of the information. In view of the uncertainties, even

* Present address: Brandenburger Str. 9, D-3250 Hameln 13/Tündern, West Germany.

† Author to whom correspondence should be addressed.

0022-4596/85 $3.00

TABLE I

X-RAY AND NEUTRON DIFFRACTION STUDIES OF SOME MEMBERS OF THE SERIES Ce_nO_{2n-2}

Phase O/Ce	Author(s)/Ref.	Crystal data	Remarks
β (1.8333)	Sørensen (*5*)	Monoclinic, isostructural with Pr_6O_{11}	High-temperature X-ray diffraction, O/Ce not determined
δ 1.818	Anderson and Wuensch (*11*)	bcc, IA3, a = 10.999 Å, isostructural with C-Ce_2O_3	Single-crystal X-ray diffraction
δ 1.812–1.804	Bevan (*12*)	Rhombohedral (pseudohexagonal, a = 3.890 Å, c = 9.538 Å)	Powder X-ray diffraction
δ 1.817	Ray *et al.* (*13*)	Characteristic peaks from neutron diffraction, no data	
ε 1.80	Height and Bevan (*14*)	Triclinic, different from $Pr_{10}O_{18}$	Annealing 430 days at 375°C
ε 1.803	Ray *et al.* (*13*)	Characteristic peaks from neutron diffraction, no data	
ζ 1.785	Bevan (*12*)	Rhombohedral (pseudohexagonal, a = 3.91 Å, c = 9.502 Å)	Powder X-ray diffraction
ζ 1.778	Height and Bevan (*14*)	Triclinic distortion of the fluorite-type pseudocell, different from Pr_9O_{16}	Annealing 180 days at 375°C
1.778	Anderson and Wuensch (*11*)	Two-phase intergrowth of δ and ι	Single-crystal X-ray diffraction
ζ 1.770	Ray *et al.* (*13*)	Characteristic peaks from neutron diffraction, no data	
ι 1.714	Anderson and Wuensch (*11*)	Hexagonal, $P6_3mmc$, a = 3.29 Å, c = 5.89 Å	Single-crystal X-ray diffraction
ι 1.722–1.710	Bevan (*12*)	Rhombohedral (pseudohexagonal, a = 3.921 Å, c = 9.637 Å) and associated superstructure lines	Powder X-ray diffraction
ι 1.714	Height and Bevan (*14*)	Rhombohedral (pseudohexagonal, a = 10.341 Å, c = 9.6668 Å)	
ι 1.714	Ray and Cox (*10*)	**Rhombohedral**, a = 6.79 Å, α = 99.4°, space group $R\bar{3}$ (pseudohexagonal, a = 10.37 Å, c = 9.67 Å), isostrucural with Pr_7O_{12} and Tb_7O_{12}	Neutron diffraction

contradictions, apparent in these results it was decided to apply the electron optical techniques to CeO_x–O_2 that have proved so powerful in sorting out the complexities of the analogous PrO_x and TbO_x systems.

Experimental

The preparation of single crystals. Single crystals of CeO_2 were prepared from CeO_2 powder (99.9%, Koch-Light, Colnbrook, England) in a flux of sodium tetraborate (99.5%, Aldrich, Milwaukee, Wisc.) (*15*). About 8 g of CeO_2 and 100 g of $Na_2B_4O_7$ were mixed in a platinum crucible covered with a platinum lid. The crucible was heated for 3 days to 1150°C, cooled to 800°C at the rate of 5°C/hr, then removed from the furnace. After dissolving the flux in hot water, the clear, colorless crystals were filtered from the solution, washed, and dried at about 150°C. The crystals were irradiated in a reactor operating at 100 kW (thermal neutron flux $\sim 9 \times 10^{11}$ n/cm^2 sec) for 2 hr. Analysis was made on a 228.4-mg sample of flux-grown $CeO_{2-\delta}$. A standard containing 49.4 μg of sodium was irradiated at the same time. The $CeO_{2-\delta}$ specimen contained 419 ± 10 ppm of sodium.

The reduction of CeO_2 powder and single crystals. The sensitivity of reduced cerium oxides to oxygen and water vapor demands that all operations on the reduced materials be accomplished in the absence of these gases. To this end, the apparatus illustrated in Fig. 2 was constructed enabling the reduction of CeO_2 at temperatures up to

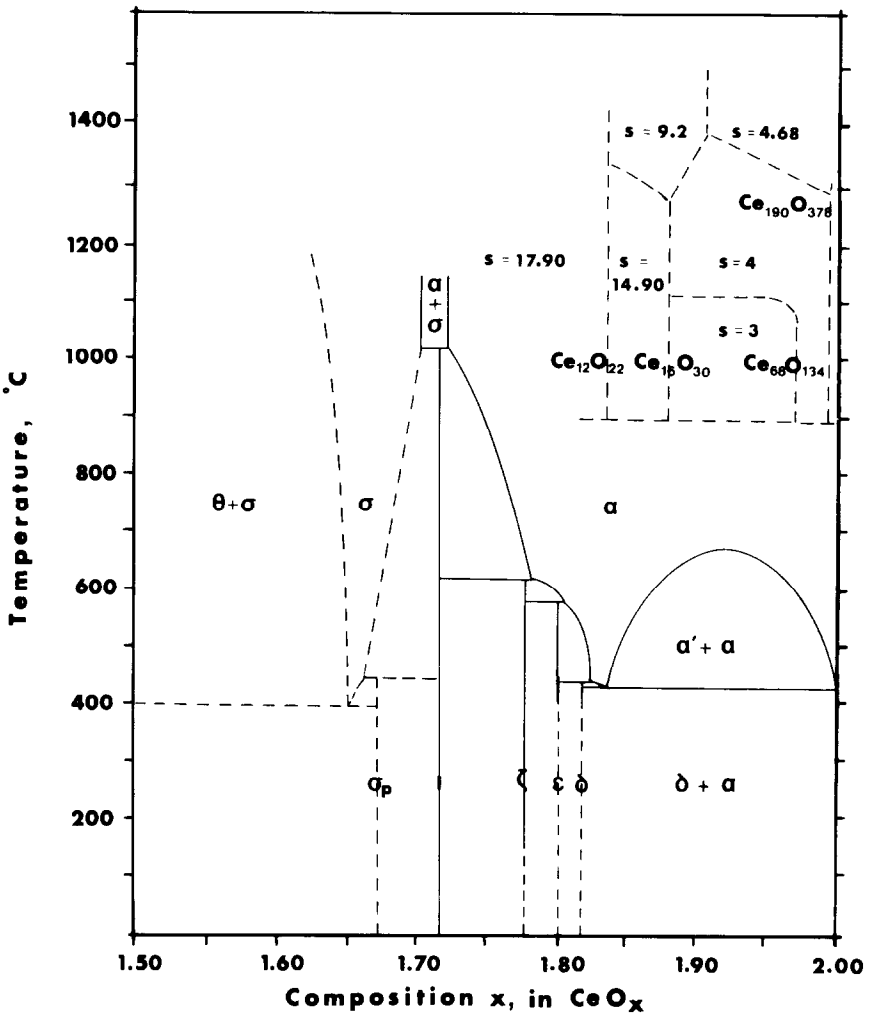

FIG. 1. Phase diagram of the CeO_x–O_2 system prior to this work. The region addressed here is in the composition range $1.714 \leq x \leq 1.818$.

1000°C in a dry hydrogen atmosphere and the covering of the reduced crystals to protect them during their removal from the reduction apparatus. Specifically, a molybdenum crucible contained the CeO_x during reduction and this could be covered with a tight-fitting iron lid by means of a magnet before removal from the apparatus (*16*). Since water is a product of the reaction and the H_2/H_2O ratio determines the fugacity of O_2 it was advantageous to maintain the pressure of H_2O at a low level, enabling the reductions to be accomplished at lower temperatures. An alumina boat containing P_2O_5 was placed in the cold end of the apparatus to maintain a low partial pressure of H_2O. Figure 3 confirms the necessity of reducing the water vapor partial pressure if one is to prepare specimens at 1000°C or below. Compare curves A and B and notice particularly (curve C) that single crystals required lower temperatures than do powders to reach the same reduced composition.

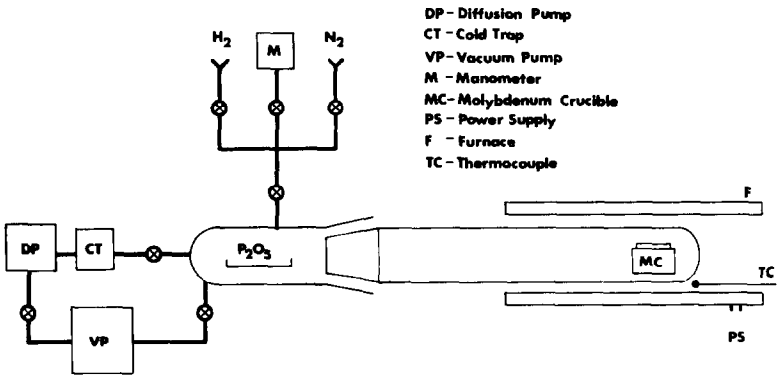

FIG. 2. The reduction apparatus for CeO_2. The specimen in MC can be sealed for removal from the apparatus. The P_2O_5 controls the H_2O pressure.

The colorless single crystals of CeO_2 that had been weighed in the capped molybdenum crucible, were exposed to H_2 in the apparatus and reduced at temperatures of 500–650°C. They became dark blue with a composition CeO_x ($1.68 \leq x \leq 2.0$). After 3 days at temperature the reaction tube was evacuated, the sample heated at about 950°C for 1–3 days and finally annealed at 350–600°C for several days. When the CeO_x crystals, contained in the molybdenum crucible, were cooled to room temperature the

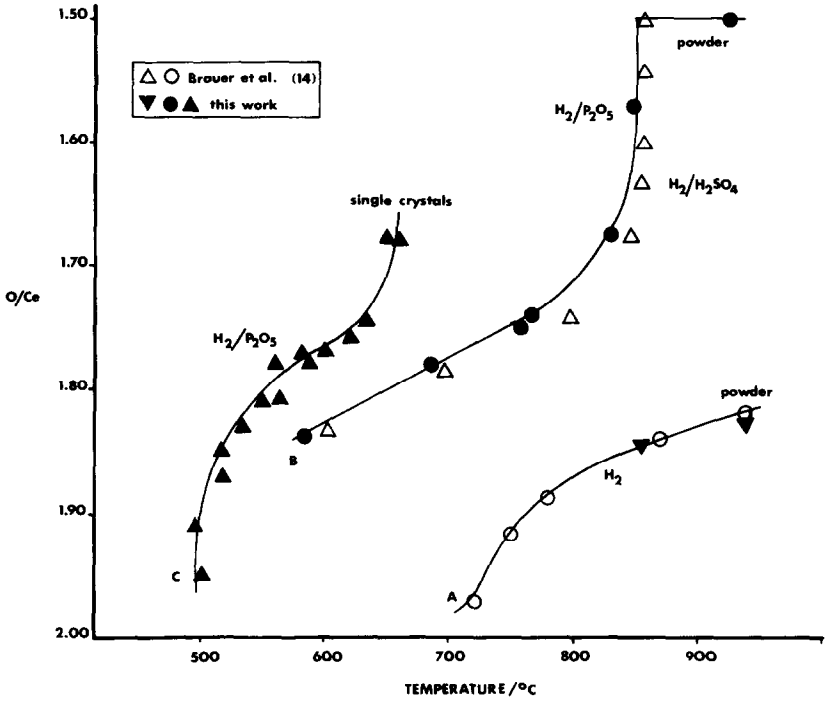

FIG. 3. The results of experiments in which cerium dioxide is reduced in hydrogen.

crucible was capped with the iron lid, weighed on a balance, and then placed in a drybox filled with N_2 desiccated by P_2O_5. It has been established that crystals undergoing treatment such as this retain their single-crystal character (*8, 11*).

Preparation of the microscope specimens for observation. All preparations of the specimen for electron microscopic examination were performed in the drybox. The dark blue crystals of CeO_x were ground in an agate mortar and placed in a small vial. The fragmented CeO_x crystals were suspended in cyclohexane (C_6H_{12}) and some transferred to a microscope grid covered with a holey carbon film as it was dipped into the suspension. The grid was then secured onto the microscope tilting specimen holder and the assembly placed into a special glass tube for transport to the microscope. Cyclohexane was dropped onto the grid supporting the CeO_x crystals to protect them from laboratory air while the tilting holder was positioned in the microscope specimen chamber and pumped down for insertion into the evacuated microscope column.

Electron microscopic observations. The reduced crystals, held on a top-entry double tilt specimen holder, were examined in a JEOL JEM 200CX microscope using axial illumination by 200-kV electrons. The general techniques used have been described previously (*18*). A dedicated computer system with its peripherals (*19*) is used to digitize and process the images obtained, calculate an image from a model structure, and compare quantitatively the observed and calculated images. The system also enables the calculation and comparison of electron diffraction patterns.

Observation of continuous reduction of CeO_x with H_2. CeO_2 (8.676 mmole) powder in a molybdenum crucible was placed in a quartz tube inside a furnace. P_2O_5 outside the furnace kept the H_2 that had been introduced relatively dry as in the reduction experiments described above (Fig. 2). The system was fitted with a mercury manometer to follow the change in H_2 pressure as the reduction proceeded and H_2 was consumed.

In order to correct for the temperature gradient in the apparatus, a hydrogen-charged system without a specimen was heated and the pressure measured over the temperature range to be studied. The extent of reaction was followed by observing the corrected H_2 pressure as a function of time. The H_2 was considered a perfect gas. The volume of the apparatus was determined to be 400 ± 5 ml.

Results and Discussion

Table II lists the oxide specimens examined in the electron microscope, the conditions of preparation, the average composition determined by weight, and the phases observed by electron diffraction. Phase designations that will be used in this discussion are as follows: σ – $Ce_2O_{3+\delta}$ (C-type), ι – Ce_7O_{12}, M13, M29, M39, M19 – $Ce_{19}O_{34}$, ζ – Ce_9O_{16}, ε – $Ce_{10}O_{18}$, δ' – $Ce_{62}O_{112}$, δ – $Ce_{11}O_{20}$, and α – $CeO_{2-\delta}$. The symbol M followed by a number indicates the multiplicity of the electron diffraction pattern relative to the fluorite subcell. A name is not suggested since in these cases the composition has not been determined unambiguously. In each case the diffraction patterns as shown in Figs. 4 or 5 are unambiguous. The disordered, nonstoichiometric σ and α phases were not of particular interest in these experiments and will not be discussed further. The presence of about 0.04% Na in the crystals is not believed to be enough to affect the conclusions drawn.

Ce_7O_{12} (iota phase). Pr_7O_{12} and Tb_7O_{12} have a fluorite-related structure whose essential defect element, a $\{135\}_{\text{Fluorite}}$ plane of six-coordinated metal atoms with the pairs of oxygen vacancies canted at a fixed angle across the plane, has been described earlier

TABLE II

PREPARATION AND DESCRIPTION OF ELECTRON MICROSCOPE SPECIMENS

Reduction		Annealing			Phases observed in the electron microscope
Temp., °C	Time, hr	Temp., °C	Time, hr	O/Ce[a]	
500	40	950	24	1.94	δ + α
		950 → 650	100		
490	20	950	110	~1.91[b]	δ + α
520	70	920	5	1.87	δ + α
		540 → 350	150		
515	65	950	24	1.85	δ + α
520	110	—	—	1.85	δ
530	40	950	100	1.83	δ
550	20	950	48	1.82	δ
		750	48		
550	90	950	240	1.81	δ + δ′
		750	48		
530	100	950	15	~1.80[b]	δ
		370	120		
570	40	950	100	1.80	δ
		950 → 650	48	1.80	δ
560	90	860	20	1.79	δ′ + M19 + M29 + M39
580	100	930	40	1.79	δ + δ′ + M13
		930 → 540			
585	24	940	48	~1.78[b]	δ + M19
		940 → 550	100		
610	65	360	70	1.78	M19
630	40	940	20	1.78	M19 + δ
		950 → 650	70		
580	65	940	120	1.77	δ
600	85	930	5	1.77	M19
		600 → 370	170		
590	70	940	24	1.76	δ + M19 + σ
		20 → 430	100		
625	70	920	15	1.76[b]	δ + M19
		380	70		
635	70	930	3	1.76	M19
		650 → 370	120		
600	90	940	4	1.75	M19
		450	15		
635	90	950	5	1.75	ι + M19 + δ
		950 → 500	48		
570	65	940	24	~1.72[b]	ι
		590	24		
645	100	930	3	1.72	ι
		600 → 370	250		
650	65	950	24	1.68	ι + σ
		950 → 600	75		

[a] Composition after annealing.

[b] Composition uncertain due to difficulties during preparation.

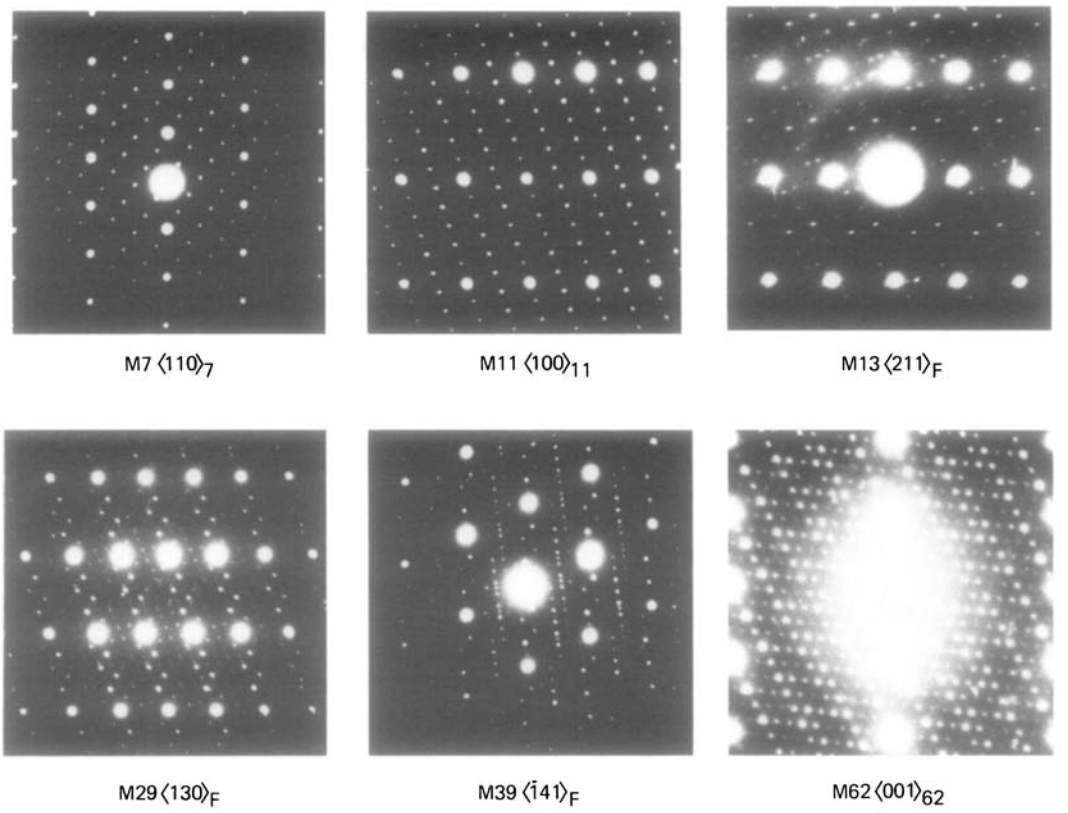

FIG. 4. Electron diffraction patterns of the phases observed in the composition range $CeO_{1.714}$–$CeO_{1.818}$ in addition to the M19 phase shown in Fig. 5. The fluorite zone designations are given where the unit cell is unknown.

(*6, 7*). This structural feature seems to be repeated either as a plane or as a buckled element in most of the known higher oxide structures of the rare earths (*1*). Figure 6 shows the known projections for M7, M11, and M19 and consistent projections for M13, M29, and M39 on $\langle 211 \rangle_F$. The X-ray and neutron diffraction studies of Ce_7O_{12} (*10, 14*) have shown it to be isostructural with Pr_7O_{12} and Tb_7O_{12}. In this study electron diffraction patterns from the $[21\bar{1}]$, $\langle 130 \rangle$, and $\langle 121 \rangle$ zones confirm that the unit cell is the same, but no images of this structure were good enough for structural confirmation. However, there is no reason to doubt that this prototype phase is isostructural in the three higher oxide systems and that the structural feature characteristic of these phases plays an important role in many of the stable phases that occur.

M19 – $Ce_{19}O_{34}$. This phase has not previsouly been reported in any of the higher rare earth oxide systems. It was observed in 10 preparations in this work as indicated in Table II. It was the only phase observed in some runs when the average composition was near $CeO_{1.78}$. (There are 19 Ce atoms in the unit cell and probably 34 oxygen atoms.) Good diffraction patterns from four different zones of these crystals were compared with those calculated from the deduced unit cell as shown in Fig. 5, as follows: $[21\bar{1}]_F = [100]_{19}$, $[\bar{1}41]_F = [010]_{19}$, $[01\bar{2}]_F = [10\bar{1}]_{19}$, and $[201]_F = [101]_{19}$. The

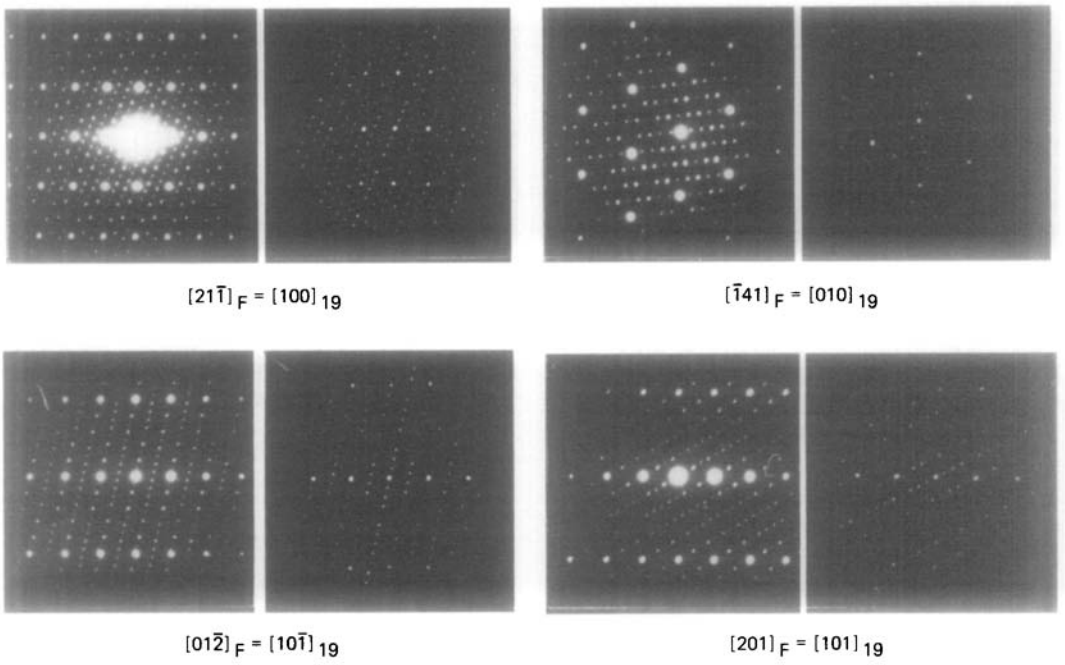

FIG. 5. Observed and calculated electron diffraction patterns for M19. The corresponding zones in the fluorite structure are indicated.

transformation matrix for M19 is

$$\begin{pmatrix} a \\ b \\ c \end{pmatrix}_{M19} = \begin{pmatrix} 1 & -1/2 & 1/2 \\ 1/2 & 2 & 1/2 \\ -1 & -1/2 & 3/2 \end{pmatrix} \begin{pmatrix} a \\ b \\ c \end{pmatrix}_{\text{fluorite}}.$$

Figure 6 contains a projection of the unit cell along $[21\bar{1}]_F$.

The projected unit cell of M19 is a remarkable assemblage of projections of known unit cell vectors in the R_nO_{2n-2} series. For example, the a-axis is the same as in R_7O_{12}. The c-axis has the same projection as the body diagonal of R_7O_{12} or the b-axis of $R_{11}O_{20}$. The b-axis could be seen variously to be the long diagonal of R_8O_{14}, or the short diagonal of $R_{12}O_{22}$, etc. However, one is tempted to emphasize the relationship between the c axis and the unit cell of R_7O_{12}. From this point of view the structure might arise from the undulating vectors $[13\bar{5}]$ and $[\bar{3}51]$ that point along $[\bar{2}84]$ much as the sequence of $[1\bar{5}3]$ followed by $[\bar{1}\bar{3}5]$ point along $[0\bar{2}2]$ and is characteristic of the even members of R_nO_{2n-2} common in PrO_x and TbO_x systems. If this is significant it

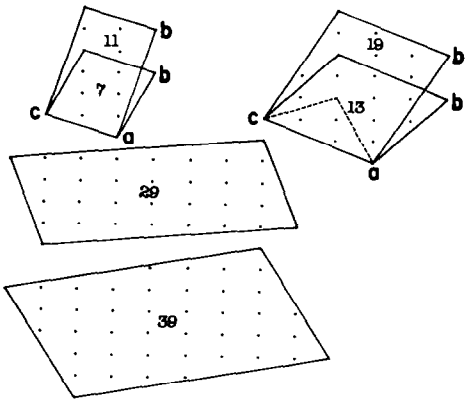

FIG. 6. Projections of the unit cells of intermediate phases along $[21\bar{1}]$ of the fluorite structure. M29 and 39 are less certain.

introduces a new planar structural feature. If the unit cell of M19 contains four oxygen vacancies, according to this viewpoint, it has a composition $Ce_{19}O_{34}$ or $CeO_{1.789}$ consistent with the average compositions of the preparations in which it is found.

Only one diffraction pattern of the hundreds taken had spots along $\langle 0\bar{2}2\rangle$ suggesting an even-*n* member of the series. This was a poor pattern without a clear indication of the multiplicity. For all practical purposes only odd-*n* members occur with any frequency in this composition interval.

M13. An electron diffraction pattern (EDP) designated M13 is shown in Fig. 4. The projected unit cell along $\langle 211\rangle_F$ is outlined in Fig. 6 where it can be compared with the projections of other unit cells known or suggested in the RO_{2-x} materials. The composition of this crystal is unknown but if it were to correspond roughly to the average composition of the preparation in which it was found it would be $Ce_{13}O_{23}$ ($CeO_{1.77}$). No diffraction pattern with a multiplicity of 13 was obtained from another zone, hence, the true unit cell is unknown. This crystal was observed when reduction was carried out at 580°C for 100 hr as listed in Table II.

M29. This phase of uncertain composition is clearly indicated by the $\langle 130\rangle_F$ diffraction pattern shown in Fig. 4. A compatible unit cell along $\langle 211\rangle_F$ is shown for comparison with other compounds in Fig. 6. If this crystal reflects the overall composition of the preparation (Table II) it would be $Ce_{29}O_{52}$ ($CeO_{1.79}$). No other crystals of multiplicity 29 were observed, hence, a unit cell cannot be obtained.

M39. Two different electron diffraction patterns were obtained from one crystal reduced at 560°C (Table II). These were along $\langle 221\rangle_F$ and $\langle \bar{1}41\rangle_F$. The latter is shown in Fig. 4. A compatible projected unit cell is shown in Fig. 6. It may be possible to determine the unit cell from these electron diffraction patterns but this has not been done. The composition might be $Ce_{39}O_{70}$ ($CeO_{1.79}$) compatible with the average composition of the preparation.

$Ce_{62}O_{112}$ (delta prime). Diffraction patterns from a number of zones of a new phase frequently seen together with the δ-phase are similar to those from the $Tb_{62}O_{112}$ (δ′) phase (*6*, *20*). The pattern shown in Fig. 4 is from the [001] zone ($[2\bar{1}0]_F$) of δ′. Many diffraction patterns with a multiplicity of 62 were observed leaving no doubt that this new phase has the same unit cell as $Tb_{62}O_{112}$. The transformation matrix is (*6*)

$$\begin{pmatrix} a \\ b \\ c \end{pmatrix}_{\delta'} = \begin{pmatrix} -1/2 & 0 & +5/2 \\ -2 & -2 & -1 \\ 2 & -1 & 0 \end{pmatrix} \begin{pmatrix} a \\ b \\ c \end{pmatrix}_{\text{fluorite}}.$$

No images of δ′ useful for structural interpretation were obtained.

$Ce_{11}O_{20}$ (delta). It is clear from Table II that diffraction patterns with a multiplicity of 11, indicating the δ-phase, were found in specimens having compositions between $CeO_{1.77}$ and $CeO_{1.94}$. In most cases two phases were found, CeO_2 when the composition was greater than $CeO_{1.85}$ and M19 when it was less. $Ce_{11}O_{20}$ was found alone at compositions of $CeO_{1.80\text{–}1.83}$. It is important to say that observations were not exhaustive since only thin edges of crystals were observed almost at random. Furthermore, the compositions were determined by weighing and there could be errors on the high composition side due to possible oxidation.

Several zones of δ were observed establishing the same unit cell as was found for δ-$Tb_{11}O_{20}$ ($Pr_{11}O_{20}$ has a different unit cell). This suggests that the structure is probably the same. Good images of δ-phase were obtained. One of these was used to compare with one calculated assuming the same structure proposed for $Tb_{11}O_{20}$ (*8*). Figure 7 is a portion of the image with two regions marked A and B. These regions were used for comparison with calculated images for

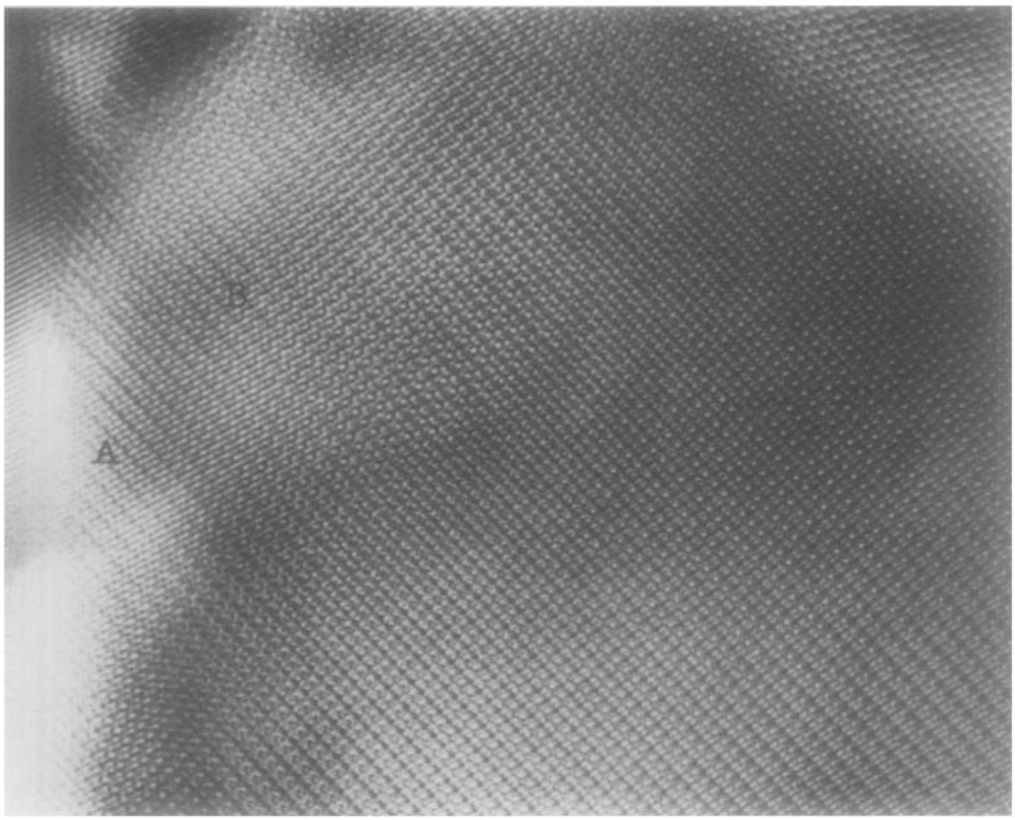

FIG. 7. An image of $Ce_{11}O_{20}$. The two regions to be averaged for the comparisons shown in Figs. 8 and 9 are marked A and B, respectively.

crystal thicknesses of 22 and 26 unit cells (6.49 Å each) thick at a defocus of −300 Å. These regions are near the edge of the crystal where the reduced phase is apparent. The comparisons are shown in Figs. 8 and 9 for regions A and B, respectively. The agreement, as indicated by the fractional mean absolute difference (FMAD) and the correlation coefficient (CC) (these would be 0 and 1, respectively, if the match were perfect) is in the range expected of a good match from previous results on known specimens (*19*). We conclude from this that the structure proposed for $Tb_{11}O_{20}$ is the same as that found for $Ce_{11}O_{20}$. The match gets significantly worse as one moves to thicker regions of the crystal as might be expected. Several other plausible models were used for image comparison with agreement outside an acceptable range.

The continuous reduction of CeO_2. It is apparent from the results indicated above that there is a discrepancy between observations made by Height and Bevan (*14*) and Ray *et al.* (*13*) as shown in Table I above. These reports indicate that Ce_9O_{16} and $Ce_{10}O_{18}$ are intermediate phases between Ce_7O_{12} and $Ce_{11}O_{20}$, whereas neither was observed in these experiments. Therefore, a slow and continuous reduction of CeO_2 by H_2 was followed in an effort to observe breaks in the reduction curve that would indicate the precise compositions of the ordered phases in this region. Breaks at com-

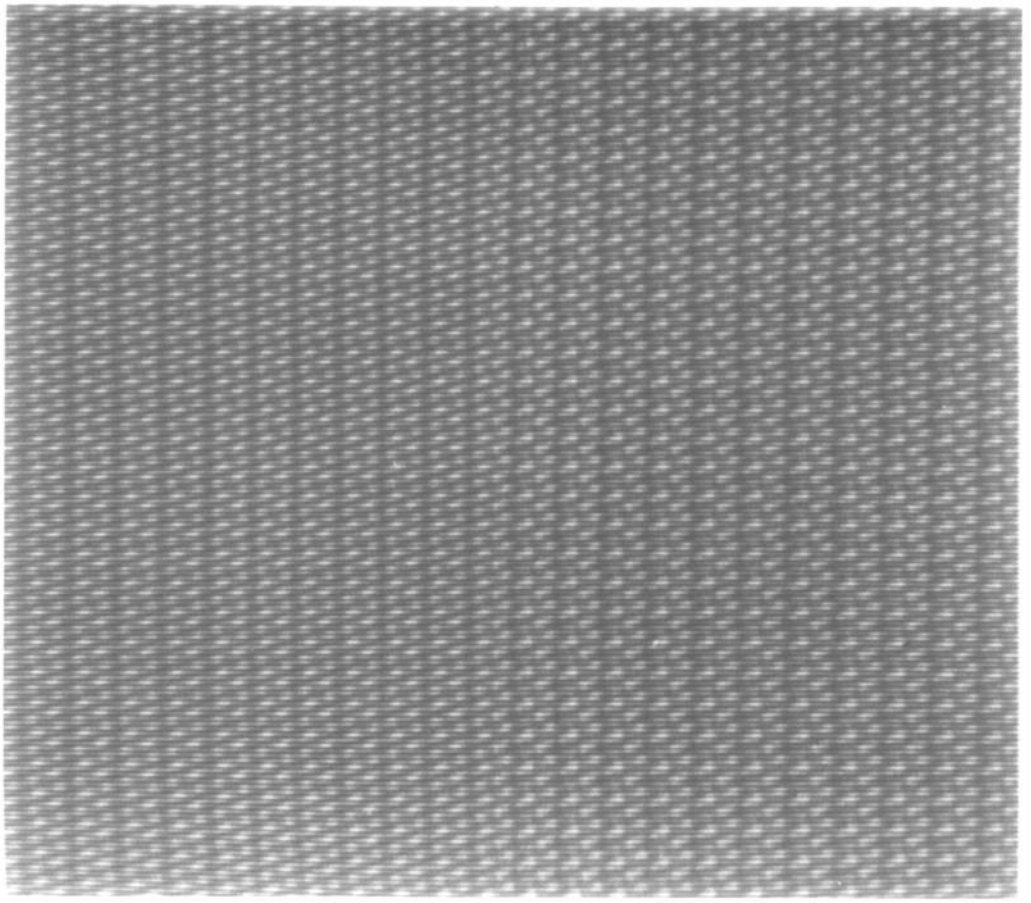

FIG. 8. A comparison of the averaged image of region A of Fig. 7 with that calculated from the proposed structure under the known conditions. The comparisons give a fractional mean average deviation of 0.080 and a correlation coefficient of 0.864 where, for a perfect fit, the numbers would be 0 and 1, respectively.

positions $CeO_{1.71}$ and $CeO_{1.82}$ were unambiguous while breaks in the interval between are inconclusive.

Conclusions

We conclude from these studies that Ce_7O_{12} is isostructural with Pr_7O_{12} and Tb_7O_{12} and with several ternary oxides with this overall metal–oxygen ratio. $Ce_{11}O_{20}$ is shown to be isostructural with $Tb_{11}O_{20}$ but quite different from the phase believed to be $Pr_{11}O_{20}$ ($Pr_{88}O_{160}$).

Three other phases in the CeO_x system previously reported, Ce_9O_{16}, $Ce_{10}O_{18}$, and $Ce_{12}O_{22}$, were not indicated in these studies. Instead, a phase $Ce_{19}O_{34}$ was observed, its unit cell determined, and a plausible structure suggested. Diffraction patterns for the phase $Ce_{62}O_{112}$ were observed in many specimens and in many zones. This appears to be isomorphous with the known phase $Tb_{62}O_{112}$, designated δ'. At least three other phases were indicated to form in this composition range.

Slow reduction of CeO_2 with hydrogen did not give an unambiguous indication of

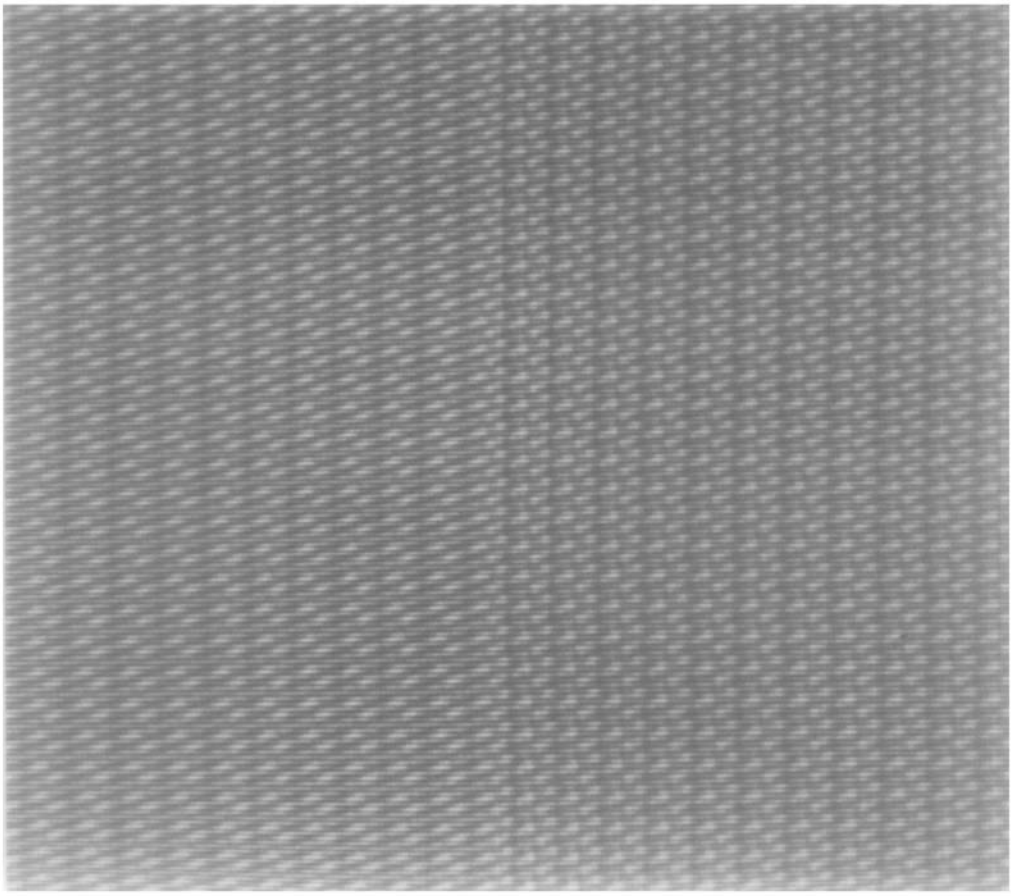

FIG. 9. A comparison of the averaged image of region B of Fig. 7 with that calculated from the proposed structure under the known conditions. The comparisons give a fractional mean average deviation of 0.089 and a correlation coefficient of 0.870 where, for a perfect fit, the numbers would be 0 and 1, respectively.

the stable compositions between $CeO_{1.71}$ and $CeO_{1.82}$, hence, one cannot say that the phases observed in this composition interval should replace or augment Ce_9O_{16} and $Ce_{10}O_{18}$ or whether there are metastabilities to be considered. Clearly, more work must be done to resolve these questions. It would be desirable to attempt to index the diffraction patterns obtained earlier by others on these new unit cells. Finally, it is becoming clear that the original simple generic formula, R_nO_{2n-2}, with $n = 7$ being the structural prototype, does not hold for some new phases observed in the rare earth oxide systems. Therefore, a more general formulation of these fluorite-related oxides is required. It is necessary to determine the structures of some key intermediate compounds, perhaps by neutron diffraction, in order to establish the interrelationships more definitely.

One striking observation is that the CeO_x intermediate phases correspond structurally much more closely to the TbO_x system than they do to that of PrO_x which should have more nearly the same metal–nonmetal radius ratio. This suggests that the sub-valence electronic similarity between Ce and

Tb, each with one electron beyond the empty or one-half-filled f orbitals, is more important than the radius ratio in determining the structure of these intermediate phases.

Acknowledgments

We are grateful for financial support by National Science Foundation Grant DMR 81-08306. The neutron activation analysis for sodium was performed by the University of Arizona, Department of Nuclear and Energy Engineering (George W. Nelson, Director) under a DOE Reactor Sharing grant. The microscope center is supported by NSF Grant DMR-8306501.

Note added in proof. After this manuscript was submitted for publication, the paper by M. Ricken *et al.* appeared in this Journal [Vol. 54, pp. 89–99 (1984)]. They measured the specific heat of CeO_{2-x} in the same composition region covered by our experiments. They observe the "known" phases Ce_nO_{2n-2} with $n = 7$, 10, and 11, but, in addition, two other phases where $2-x$ in CeO_{2-x} is 1.79 and 1.808, respectively. These last two phases would correspond exactly to our M19 and $Ce_{62}O_{112}$ (δ') phases. Furthermore, they comment (p. 97) that another peritectic line suggests a phase between 1.79 and 1.80. This could be our M29 with $CeO_{1.793}$ or M39 with $CeO_{1.795}$ or both. This obvious agreement with our results with the added observation of $CeO_{1.800}$, not seen by us, confirms the intricate complexity of CeO_{2-x} ($1.82 > 2-x > 1.71$).

References

1. L. EYRING, *in* "Handbook on the Physics and Chemistry of Rare Earths," Vol. 3 (K. A. Gschneidner, Jr. and L. Eyring, Eds.), pp. 337–399, North-Holland, Amsterdam (1979).
2. G. BRAUER AND H. GRADINGER, *Z. Anorg. Chem.* **277,** 89 (1954).
3. D. J. M. BEVAN AND J. KORDIS, *J. Inorg. Nucl. Chem.* **26,** 1509 (1964).
4. R. J. PANLENER, R. H. BLUMENTHAL, AND J. E. GARNES, *J. Phys. Chem. Solids* **36,** 1213 (1975).
5. O. T. SØRENSEN, *J. Solid State Chem.* **18,** 217 (1976).
6. P. KUNZMANN AND L. EYRING, *J. Solid State Chem.* **14,** 229 (1975).
7. R. T. TUENGE AND L. EYRING, *J. Solid State Chem.* **29,** 165 (1979).
8. R. T. TUENGE AND L. EYRING, *J. Solid State Chem.* **41,** 75 (1982).
9. R. B. VON DREELE, L. EYRING, A. L. BOWMAN, AND J. L. YARNELL, *Acta Crystallogr. Sect. B* **31,** 971 (1975).
10. S. P. RAY AND D. E. COX, *J. Solid State Chem.* **15,** 333 (1975).
11. H. T. ANDERSON AND B. J. WUENSCH, *in* "Fast Ion Transport in Solids" (W. Van Gool, Ed.), pp. 285–299, North-Holland, Amsterdam (1973).
12. D. J. M. BEVAN, *Inorg. Nucl. Chem.* **1,** 49 (1955).
13. S. P. RAY, A. S. NOWICK, AND D. E. COX, *J. Solid State Chem.* **15,** 344 (1975).
14. T. M. HEIGHT AND D. J. M. BEVAN, unpublished results.
15. A. HARARI, J. THÉRY, AND R. COLLONGUES, *Rev. Int. Hautes Temp. Refract.* **4,** 207 (1967).
16. P. KNAPPE AND H. MUELLER, *Z. Allg. Anorg. Chem.* **487,** 63 (1982).
17. G. BRAUER, K. A. GINGERICH, AND U. HOLTSCHMIDT, *J. Inorg. Nucl. Chem.* **16,** 77 (1960).
18. S. IIJIMA, *Acta Crystallogr. Sect. A* **29,** 18 (1973).
19. A. RAE SMITH AND L. EYRING, *Ultramicroscopy* **8,** 65 (1982).
20. Z. C. KANG, A. RAE SMITH, AND L. EYRING, unpublished results.